Colletodiol derivatives of the endophytic fungus Trichocladium sp.

Viktor E. Simons, Attila Mándi, Marian Frank, Lasse van Geelen, Nam Tran-Cong, Dorothea Albrecht, Annika Coort, Christina Gebhard, Tibor Kurtán, Rainer Kalscheuer

Article - Version of Record

Wissen, wo das Wissen ist.

UNIVERSITÄTS- UND LANDESBIBLIOTHEK DÜSSELDORF

Colletodiol derivatives of the endophytic fungus *Trichocladium* sp.

Viktor E. Simons [a], Attila Mándi [b], Marian Frank [a], Lasse van Geelen [a], Nam Tran-Cong [a], Dorothea Albrecht [a], Annika Coort [a], Christina Gebhard [a], Tibor Kurtán [b], Rainer Kalscheuer [a],*

[a] *Heinrich Heine University Düsseldorf, Faculty of Mathematics and Natural Sciences, Institute of Pharmaceutical Biology and Biotechnology, Universitätsstrasse 1, Düsseldorf 40225, Germany*
[b] *Department of Organic Chemistry, University of Debrecen, P.O. Box 400, Debrecen 4002, Hungary*

A B S T R A C T

The OSMAC (one strain many compounds) concept is a cultivation-based approach to increase the diversity of secondary metabolites in microorganisms. In this study, we applied the OSMAC-approach to the endophytic fungus *Trichocladium* sp. by supplementation of the cultivation medium with 2.5% phenylalanine. This experiment yielded five new compounds, trichocladiol (**1**), trichocladic acid (**2**), colletodiolic acid (**3**), colletolactone (**4**) and colletolic acid (**5**), together with five previously described ones (**6–10**). The structures were elucidated via comprehensive spectroscopic measurements, and the absolute configurations of compound **1** was elucidated by using TDDFT-ECD calculations. For formation of compounds **3–5**, a pathway based on colletodiol biosynthesis is proposed. Compound **6** exhibited strong antibacterial activity against methicillin-resistant *Staphylococcus aureus* with a minimal inhibitory concentration (MIC) of 0.78 μM as well as a strong cytotoxic effect against the human monocytic cell line THP1 with an IC_{50} of 0.7 μM. Compound **8** showed moderate antibacterial activity against *Mycobacterium tuberculosis* with a MIC of 25 μM and a weak cytotoxic effect against THP1 cells with an IC_{50} of 42 μM.

1. Introduction

Since the early 20th century, microorganisms derived from natural samples became a promising source for novel bioactive compounds. The isolation and characterization of penicillin in 1929 by Alexander Fleming marked the beginning of a new era of natural product-based drug discovery [1]. In 1940, Waksman and Woodruff firstly described soil microorganisms able to inhibit the growth of pathogenic bacteria and isolated the peptide antibiotic actinomycin [2]. This was the beginning of a prolific area of discovery of bioactive natural compounds from soil-derived microorganisms. The isolation of taxol from the endophytic fungus *Taxomyces andreanae* in 1993 then shed light onto endophytic microorganisms and showed a glimpse of their potential as a promising source of bioactive secondary metabolites [3]. Endophytic microorganisms live in a symbiotic relationship with their plant host and are able to release antibiotics and other compounds as a defense mechanism [4]. Previously studied plant species mostly contain at least one microbe, and growth in unique environmental surroundings often lead to the discovery of novel endophytes. Thus, the given opportunities for the isolation of promising microorganisms from plants are manifold

[4,5]. Under laboratory cultivation conditions, many biosynthetic gene clusters (BGCs) of microbes are not expressed in axenic cultures. This led to different approaches trying to activate these silent genes in order to isolate new cryptic metabolites [6]. A cultivation-based concept termed OSMAC (**O**ne **S**train **Ma**ny **C**ompounds) was described by Bode et al. in 2002 where even small changes in the cultivation conditions such as modification of the cultural medium, temperature or the introduction of co-cultivation attempts are able to activate silent gene clusters and thus can result in the discovery of new natural products [7]. Previous work has indicated that the endophytic fungus *Trichocladium* sp. is amenable to trigger secondary metabolism by the OSMAC approach [8]. Building upon this observation, we now extended the OSMAC concept to an axenic culture of *Trichocladium* sp. by enrichment of solid rice medium with the amino acid ʟ-phenylalanine. This fermentation yielded ten natural compounds including five new compounds (**1–5**) and five already described ones (**6–10**). The two macrolides colletoketol and colletodiol were isolated previously from cultures of *Trichocladium* sp. [8]. Compounds **3–5** now seem to represent intermediates or alternative metabolites of the fungal biosynthesis pathway for these macrolides. The molecular structures of the compounds **1–10** were elucidated using

* Corresponding author.
  E-mail address: rainer.kalscheuer@hhu.de (R. Kalscheuer).

high-resolution electrospray ionization mass spectrometry (HRESIMS) combined with 1D- and 2D-NMR measurements. The absolute configuration for compound **1** was determined on the basis of ECD calculations. All isolated compounds were tested for their antimicrobial activity against the human pathogens *Staphylococcus aureus* ATCC 700699, *Pseudomonas aeruginosa* ATCC 87110, *Candida albicans* ATCC 24433 and *Mycobacterium tuberculosis* ATCC 27294, and for their cytotoxic activity against the THP1 human cell line.

2. Results and discussion

During our ongoing investigation of the endophytic fungus *Trichocladium* sp. HCRSW, which was isolated from roots of the Vietnamese plant *Houttuynia cordata*, we have already reported on the isolation of natural compounds resulting from an OSMAC-approach employing L-tryptophane feeding as well as from a fungal-bacterial co-cultivation experiment [8]. We now present the results of an additional OSMAC experiment employing 2.5% (w/v) L-phenylalanine supplementation to solid rice medium. HPLC-DAD chromatographic comparison of ethyl-acetate (EtOAc) extracts of the phenylalanine cultures to the control cultures revealed the presence of formerly undetected secondary metabolites in the semi-polar range. Chromatographic workup of the extract resulted in the isolation of the five known compounds chaeto-chromin A (**6**) [9], phenazine-1-carboxylic acid (**7**) [10], phenazine-1-carboxamide (**8**) [11], dechlorodihydromaldoxin (**9**) [12] and fuscoa-tramide (**10**) [13], as well as of five new compounds including a new dihydronapthalenone compound (**1**), a new macrocarpon [14] derivative (**2**) and three new open chain derivatives (**3–5**) of the macrocyclic dilactones colletol [15] and colletodiol [16]. Colletodiol itself is a direct precursor of the antibiotic grahamimycin A1 [17], which is equal to colletoketon. Interestingly, compounds **3–5** are structurally closely related monoesters to colletodiol and dilactonic derivatives. The planar structures of all isolated compounds were unequivocally elucidated based on NMR and MS spectral data, and their bioactivity against several pathogenic microorganisms and the human THP1 cell line was investigated. The absolute configuration of compound **1** was determined by TDDFT-ECD calculations. We present the structure elucidation of new compounds **1–5** together with a proposal of a pathway to build

compounds **3–5** (Fig. 1).

2.1. Structure elucidation

2.1.1. Structure elucidation of compound **1**

Compound **1** was isolated as a yellowish solid and showed UV absorption maxima at 219 and 291 nm. Its molecular formula was assigned as $C_{11}H_{12}O_5$ based on its HRESIMS pseudomolecular ion peak at 225.0756 m/z (calcd. For $C_{11}H_{13}O_5$) with six degrees of unsaturation.

Table 1
NMR data for **1** (measured in DMSO-d_6, MeOH-d_4 and acetone-d_6 at 150 Hz and 600 MHz, respectively).

Position	δ_C* DMSO-d_6	δ_H, m (J in Hz) DMSO-d_6	δ_H, m (J in Hz) MeOH-d_4	δ_C Acetone-d_6	δ_H, m (J in Hz) Acetone-d_6
1	201.2, C			201.7, C	
2	43.1, CH$_2$	2.80, dd (17.2, 3.4) 2.66, dd (17.2, 5.8)	2.88, dd (17.2, 3.9) 2.77, dd (17.2, 7.4)	43.7, CH$_2$	2.83, d (3.6)
3	69.0, CH	4.11, m	4.20, ddd (7.4, 3.9, 2.9)	70.3, CH	4.29, br s
3-OH		4.94, d (4.1)			4.12, d (4.6)
4	68.9, CH	4.61, dd (6.7, 2.0)	4.70, d (2.9)	70.8, CH	4.77, br s
4-OH		5.38, d (6.7)			4.41, d (6.7)
4a	144.6, C			144.8, C	
5	105.8, CH	6.61, br s	6.58, s	107.4, CH	6.72, s
6	162.9, C			163.6, C	
6-OH		10.56, br s			9.38, br s
7	108.5, C			111.0, C	
8	162.0, C			163.6, C	
8-OH		13.03, s			13.09, s
8a	108.5, C			111.5, C	
9	6.9, CH$_3$	1.93, s	2.02, s	7.5, CH$_3$	2.03, s

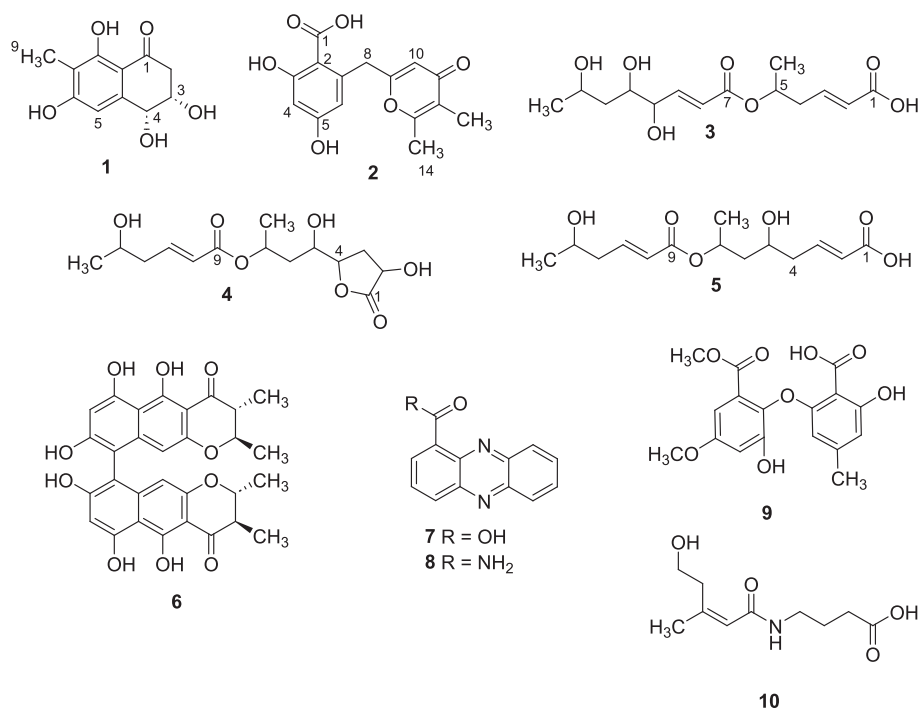* Signals were extracted from HSQC and HMBC spectra.

Fig. 1. Structures of isolated compounds from *Trichocladium* sp. resulting from OSMAC approach with 2.5% n(w/v) L-phenylalanine.

When analyzing the ^{1}H- and ^{13}C-spectra (Table 1, Fig. 2), the presence of a strongly deshielded, chelated δ 13.03 ppm (OH-8) and non-chelated phenol δ 10.56 ppm (6-OH), one aromatic singlet δ 6.61 ppm (H-5) and one aromatic methyl singlet δ 1.93 ppm (CH$_3$–9) suggested the presence of a pentasubstituted phenyl ketone unit. This was confirmed by detailed analysis of the HMBC correlation from H-5 to quaternary C-7 (δ 108.5 ppm), C-8a (δ 108.5 ppm) and C-4a (δ 144.6 ppm) and from chelated OH-8 to adjacent quaternary C-8 (δ 162.0 ppm), C-7 and C-8a. The relative configuration can be accessed through the NOESY measurement. Since the H-3 (δ 4.29 ppm, acetone-d_6) and H-4 protons (δ 4.77 ppm, acetone-d_6) give NOE correlation and the vicinal coupling constant $^3J_{H-3,H-4}$ has a small value (2.9 Hz in MeOH-d_4), they have *cis* relative configuration. Compound **1** contains a tetralone (3,4-dihydronaphthalen-1(2H)-one) moiety, which similarly to chroman-4-one and dihydroisocoumarin derivatives have a cyclic aryl ketone chromophore. For chroman-4-ones and dihydroisocoumarins, a helicity rule correlates the helicity of the heteroring and the sign of the n-π* Cotton effect (CE), according to which *P* helicity of the heteroring adopting envelope conformation is manifested in a positive n-π* CE [18–21]. In the case of chiral non-racemic tetralones, there is no straightforward general correlation between the sign of the n-π* CE and conformation of the non-aromatic ring. For most of the reported examples, *M*-helicity belonged to positive n-π* CE [20,22–25], but there were also cases when the *P*-helicity ring produced a positive n-π* CE [24–27]. The position and nature of the substituents may play a non-negligible role in the helicity rule. For instance, the intramolecular hydrogen bonding of the 8-OH group with the carbonyl oxygen results in a hypsochromic shift of the n-π* transition from >310 nm to <300–290 nm, which can change the order of the n-π* and π-π* transitions [22,26]. Thus it is highly recommended to perform conformational analysis and TDDFT-ECD calculations to avoid wrong configurational assignments [18].

Conformational analysis of (3*R*,4*S*)-**1** resulted in 16 MMFF conformers, the ωB97X/TZVP PCM/MeOH re-optimization of which yielded 12 low-energy conformers above 1% Boltzmann population (supplementary materials **Fig. S1**) [28,29]. Boltzmann-averaged ECD spectra computed at various levels of theory gave nice mirror-image spectra of the experimental ECD spectrum (Fig. 3). Furthermore, the first 6 conformers including both *M*- and *P*-helicity conformers had similar ECD spectra allowing a solid elucidation of the absolute configuration as (3*S*,4*R*). The n-π* transition was identified as the second transition at around 285 nm, which was due to the hydrogen bonding of the carbonyl oxygen with the 8-OH group (Figs. 4, 5 and supplementary materials **Fig. S2**). Our results suggested that there is no clear correlation between the helicity of the carbocyclic ring and the sign of the n-π* CE in **1**. Conformers A and E had *M*- and *P*-helicity with envelop conformation, respectively, but both of them had positive computed CE for the n-π* CE
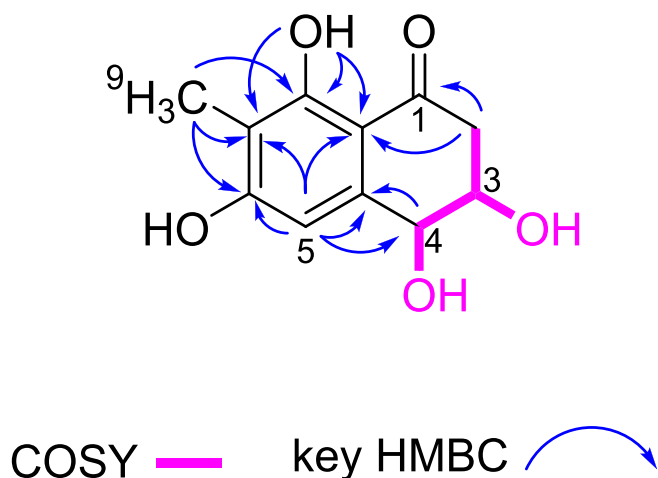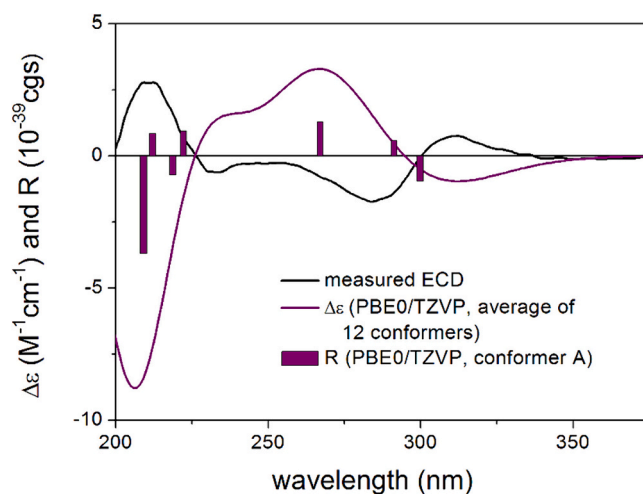

Fig. 3. Comparison of the experimental ECD spectrum of **1** measured in MeOH with the PBE0/TZVP PCM/MeOH spectrum of (3*R*,4*S*)-**1** (level of optimization: ωB97X/TZVP PCM/MeOH). The bars represent the rotational strength values of the lowest-energy conformer.
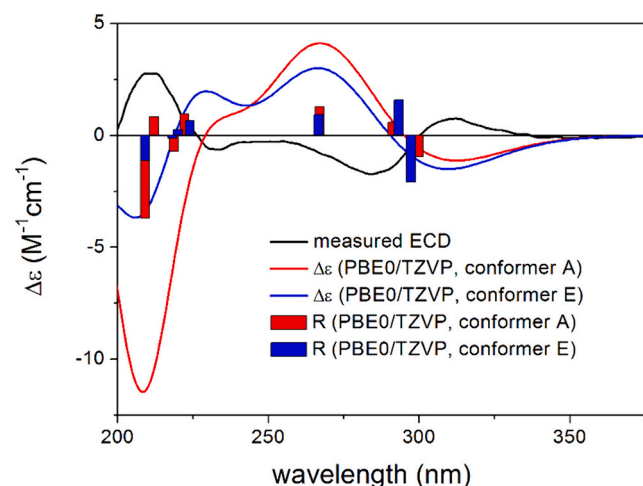

Fig. 4. Comparison of the experimental ECD spectrum of **1** measured in MeOH with the PBE0/TZVP PCM/MeOH spectra of the lowest-energy conformers with *M*- (red) and *P*-helicity (blue) of (3*R*,4*S*)-**1** (level of optimization: ωB97X/TZVP PCM/MeOH). The bars represent the rotational strength values of the corresponding conformers. (For interpretation of the references to colour in this figure legend, the reader is referred to the web version of this article.)

at 285 nm.

2.1.2. Structure elucidation of compound **2**

Compound **2** was isolated as a white powder and showed UV absorption maxima at 256 and 300 nm. The molecular formula was assigned as C$_{15}$H$_{14}$O$_6$ based on its HRESIMS pseudomolecular ion peak at 291.0866 *m/z* (calcd. For C$_{15}$H$_{15}$O$_6$) with nine degrees of unsaturation. Analysis of the ^{1}H NMR spectrum (Table 2, Fig. 6) showed strongly deshielded aromatic OH-groups with δ 10.14 ppm (3-OH) and 13.22 ppm (1-OH), three aromatic protons H-4 (δ 6.20 ppm), H-6 (δ 6.20 ppm) and H-10 (δ 5.67 ppm), a methylenic group H-8 (δ 4.11 ppm) and two methyl groups H-14 (δ 2.24 ppm) and H-15 (δ 1.77 ppm). Analysis of the HMBC correlations of the three aromatic protons revealed H-4 and H-6 being meta-positioned in a tetrasubstituted phenyl group, while H-10 is positioned in a different aromatic ring system. HMBC correlations from H-8 to C-10 (δ 110.9 ppm), C-2 (δ 106.4 ppm) and C-6 (δ 110.9 ppm) highlighted H-8 being a methylene group connecting two aromatic ring

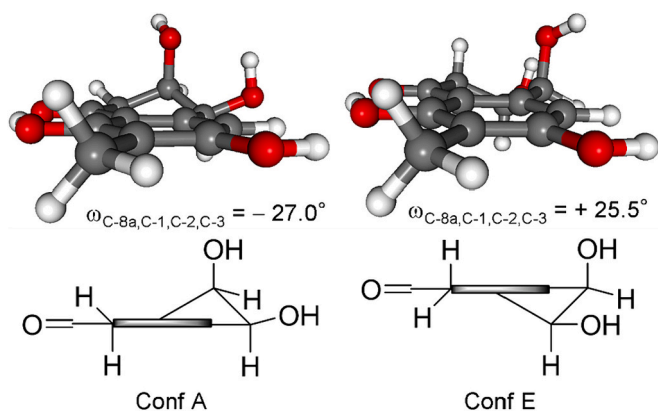**Fig. 2.** Key NMR correlations for **1**.

Fig. 5. Side-view (up) and projecting view (down) of the lowest-energy *M*-(left) and *P*-helicity (right) conformers of (3*R*,4*S*)-**1** (level of optimization: ωB97X/TZVP PCM/MeOH).

Table 2
NMR data for **2** (measured in DMSO-d_6 at 150 Hz and 600 MHz, respectively).

Position	δ_C*	δ_H, m (J in Hz)
1	172.4, C	
2	106.4, C [108.48]	[6.22, d]
3	164.2, C [159.94]	
4	101.6, CH [102.44]	6.20, br s 2H [6.2, t]
5	161.6, C [159.94]	
6	110.9, CH [108.48]	6.20, br s 2H [6.22, d]
7	139.0, C [138.69]	
8	38.2, CH$_2$ [40.49]	4.11, s [3.72, s]
9	167.7, C [169.94]	
10	110.9, CH [112.68]	5.67, s [6.14, s]
11	178.3, C [182.37]	
12	119.6, C [121.28]	
13	161.3, C [164.82]	
14	17.4, CH$_3$ [17.74]	2.24, d (0.9) [2.35, s]
15	9.3, CH$_3$ [9.68]	1.77, d (0.9) [1,92, s]
1-OH		13.22, br s
3-OH		10.14, s

* Signals were extracted from HSQC and HMBC spectra. Values in square brackets show the respective published δ of chaetosemin J [30] for comparison.
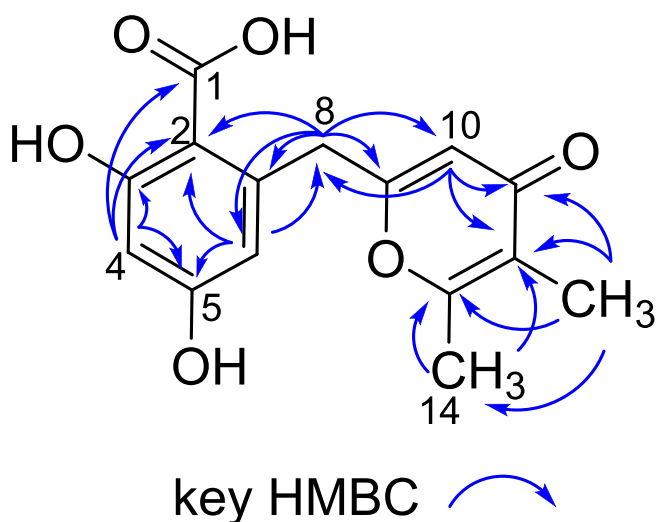

Fig. 6. Key NMR correlations for **2**.

systems. HMBC correlations from H-4 to C-1 (δ 172.4 ppm), C-2 and C-3 (δ 164.2 ppm), H-5 to C-2 and C-5 (δ 161.6 ppm) and H-8 to C-2, C-6 and C-7 (δ 139.0 ppm) revealed the structure of a dihydroxybenzoic acid

moiety, while HMBC correlations from H-8 to C-9 (δ 167.7 ppm) and C-10, from H-10 to C-11 (δ 178.3 ppm) and C-12 (δ 119.6 ppm), from H-14 to C-12 and C-13 (δ 161.3 ppm) and adjacent H-15 to C-11, C-12, C-13 and C-14 (δ 17.4 ppm) elucidated the structure of a dimethyl-pyranone. The observed signals were in good agreement with the ^{1}H and ^{13}C NMR resonance spectra reported for chaetosemin *J* (Table 2), a polyketide isolated from the ascomycete *Chaetomium seminudum* [30]. The reported structure of chaetosemin *J* is identical to that of compound **2** only differing by lack of the carboxylic acid group at position 2 (Figs. 1, 6).

2.1.3. Structure elucidation of compound 3

Compound **3** was isolated as a yellowish oil and showed only one UV absorption maximum at 218 nm near the solvent cut-off. The molecular formula was assigned as $C_{14}H_{22}O_7$ based on its HRESIMS pseudomolecular ion peak at 303.1439 *m/z* (calcd. For $C_{15}H_{23}O_7$) with four degrees of unsaturation. Detailed analysis of ^{1}H NMR, ^{13}C NMR, COSY and HSQC spectra (Table 3) revealed two distinct spin systems starting from an *E*-double bond (H-2/H-3 and H-8/H-9) connected to an oxygenated alkyl chain ending in a terminal methyl moiety each. The *E*-double bonds both exhibit asymmetrically deshielded protons (H-2/H-8: 5.8–6.0 ppm and H-3/H-9: 6.7–7.0 ppm) suggesting an adjacent carbonyl moiety. Furthermore, investigation of the HMBC spectrum revealed these two carbonyl moieties to be esters or carboxylated by observing the correlation of H-3 (δ_H 6.74 ppm) to C-1 (δ_C 166.9 ppm) and H-9 (δ_H 6.97 ppm) to C-7 (δ_C 165.2 ppm). With this information, COSY, HSQC and HMBC revealed two scaffold subunits. Carbons C-1 to C-6 formed a hex-2-enoic acid substructure with an oxygenated position CH-5 (δ_H 4.99 ppm, δ_C 68.9 ppm) and C-7 to C-14 formed an oct-2-enoic acid substructure with oxygenated positions CH-10 (δ_H 4.12 ppm, δ_C 72.8 ppm), CH-11(δ_H 3.61 ppm, δ_C 71.5 ppm) and CH-13(δ_H 3.78 ppm, δ_C 64.5 ppm). Connection of these subunits was determined to be through an ester bond between position CH-5 and carboxyl C-7 based on HMBC correlation from H-5 to C-7 and the stronger relative deshielding of H-5 (δ_H 4.99 ppm) when compared to other oxygenated methin protons (δ_H < 4.12 ppm) in the molecule. The remaining oxygenated methins where determined to be hydroxyl moieties based on the calculated molecular formula, as there were no missing degrees of unsaturation. Thus, the planar structure of **3** was elucidated as shown in Fig. 7. The compound may be interpreted as a linear non-lactonized precursor to colletodiol [31], which has been isolated from this fungal strain before [8].

2.1.4. Structure elucidation of compounds 4 and 5

Compound **4** was isolated as a colorless oil and showed only one UV absorption maximum at 218 nm near the solvent cutoff. Its molecular formula was determined as $C_{14}H_{22}O_7$ with four degrees of unsaturation. This was based on the HRESIMS signals of the pseudomolecular ion at 303.1442 *m/z* and ammonium adduct at 320.1708 *m/z*, which

Table 3
NMR data for **3** (measured in DMSO-d_6 at 150 Hz and 600 MHz, respectively).

Position	δ_C	δ_H, m (J in Hz)
1	166.9, C	
2	124.6, CH	5.83, dt (15.6, 1.5)
3	143.7, CH	6.74, dt (15.6, 7.3)
4	37.6, CH$_2$	2.48, m 2H
5	68.9, CH	4.99, m
6	19.6, CH$_3$	1.21, d (6.3) 3H
7	165.2, C	
8	120.0, CH	5.96, dd (15.7, 1.9)
9	150.1, CH	6.97, dd (15.7, 4.1)
10	72.8, CH	4.12, m
11	71.5, CH	3.61, dt (9.4, 4.0)
12	41.0, CH$_2$	1.42, ddd (13.6, 6.3, 3.7) 1.35, ddd (13.6, 9.4, 6.7)
13	64.5, CH	3.78, m
14	23.4, CH$_3$	1.04, d (6.2) 3H
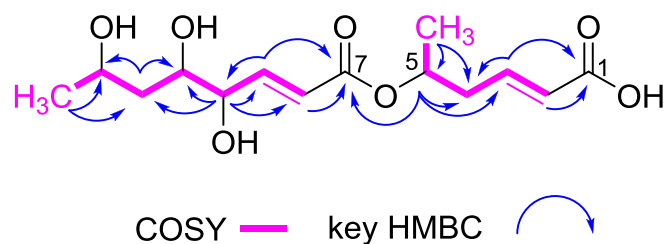
Fig. 7. Key NMR correlations for **3**.

calculated for $C_{14}H_{23}O_7$ and $C_{14}H_{26}NO_7$, respectively. Analysis of the ^1H and ^{13}C NMR spectra (Table 4) revealed a high degree of similarity to **3**. The common substructure was revealed to be a similar oxygenated hex-2-enoic acid subunit with *E* configuration (*J* 15.6 Hz) between CH-10 (δ_H 5.85 ppm, δ_C 122.7 ppm) and CH-11 (δ_H 6.89 ppm, δ_C 146.6 ppm). The major difference compared to **3** was the relative shielding (-1.24 ppm) of the oxygenated methin CH-13 (δ_H 3.74 ppm, δ_C 65.0 ppm) and the presence of hydroxyl 13-OH (δ_H 4.67 ppm), which was detectable via COSY correlation to H-13. This confirmed the connection to the remaining molecule to be established through an ester bond via carbonyl C-9 (δ_C 165.0 ppm) rather than through a hydroxyl function as in **3**. Detailed analysis of the COSY spectrum revealed that the remaining signals all belonged to a single second spin system starting from a terminal methyl CH_3-8 (δ_H 1.22 ppm), which is connected to a series of oxygenated methin protons CH-7 (δ_H 5.04 ppm), CH-5 (δ_H 3.51 ppm), CH-2 (δ_H 4.45 ppm) and methylene units CH_2-3 (δ_H 2.38/1.87 ppm), CH_2-6 (δ_H 1.78/1.59 ppm), ending in a tertiary alcohol 2-OH (δ_H 5.19 ppm). Analysis of the HMBC spectrum revealed the connection to the *(E)*-5-hydroxyhex-2-enoic acid subunit through ester bond with oxygenated methin CH-7 via correlation from H-7 to C-9, as well as the deshielded chemical shift of H-7 compared to the remaining oxygenated

methin units (δ_H 5.04 ppm). Furthermore, HMBC correlations from H-2 and H-3 revealed an adjacent carbonyl C-1 (δ_C 177.0 ppm) with unusually strong deshielding, suggesting incorporation into a five membered ring system. This ring system was established as a lactone bond between carboxylate C-1 and oxygenated methin C-4 (δ_C 78.3 ppm) which is in agreement with the unusually strong deshielding of both carbons. The position of the hydroxyl moiety 5-OH (δ_H 5.19 ppm) was unequivocally determined via COSY correlation to H-5. Thus, all signals and degrees of unsaturation were assigned and the planar structure of **4** was elucidated as shown in Fig. 8. The proposed structure reflects the same biosynthetic building blocks for colletodiol as **3** with a reversed order of the hex-2-enoic acid and oct-2-enoic acid. Additionally, a water molecule was added to the *E* double bond of the oct-2-enoic acid, thus removing the stereochemical obstacle and allowing for intramolecular lactonization to take place.

Compound **5** was isolated as a colorless oil and exhibited one UV absorption maximum at 219 nm near the solvent cutoff. The molecular formula was determined to be $C_{14}H_{22}O_6$ based on the HRESIMS pseudomolecular ion signal at 287.1492 *m/z* and ammonium adduct ion signal at 304.1759 m/z, which were calculated for $C_{14}H_{23}O_6$ and $C_{14}H_{26}NO_6$, respectively. This molecular formula suggested **5** to be a desoxy derivative of **3** or **4**. Comparison of ^1H-, ^{13}C NMR, COSY, HSQC and HMBC spectra of **5** (Table 4) with those of **3** and **4** revealed that **5** contains a terminal *(E)*-5-hydroxyhex-2-enoic acid subunit identical to the one expressed in **4** with proton chemical shifts differing <0.1 ppm and carbon chemical shifts <0.4 ppm. Analysis of COSY for the remaining signals revealed a singular additional spin system consisting of an *E* double bond (*J* 15.7 Hz) between H-2 (δ_H 5.66 ppm) and H-3 (δ_H 6.66 ppm), followed up by alternating methylene CH_2-4 (δ_H 2.37/2.26 ppm), CH_2-6 (δ_H 1.78/1.54 ppm) and oxygenated methin protons CH-5 (δ_H 3.37 ppm), CH-7 (δ_H 4.76 ppm) and ending in a terminal methyl unit CH_3-8 (δ_H 1.17 ppm). Analysis of HMBC correlations from H-3 revealed carboxylic C-1 (δ_C 167.2 ppm), and the connection to the *(E)*-5-hydroxyhex-2-enoic acid subunit via ester bond was established based on the HMBC correlation of H-7 to C-9 (δ_C 165.1 ppm), as well as the strongly deshielded chemical shift of H-7. Furthermore, the position of hydroxyl unit 5-OH (δ_H 4.71 ppm) was ascertained based on its COSY correlation to H-5, thus unequivocally confirming the second part of the structure to be a *(E)*-7, 5-dihyroxy-oct-2-enoic acid. Thus, the planar structure of **5** was elucidated as shown in Fig. 8.

2.2. Determination of antibacterial activity

Compounds **1–10** were tested in a minimal inhibitory concentration assay against methicillin resistant *Staphylococcus aureus* ATCC 700699 (MRSA), *Pseudomonas aeruginosa* ATCC 87110, *Candida albicans* ATCC 24433 and *Mycobacterium tuberculosis* ATCC 27294. None of the new compounds (**1–5**) showed inhibition against the pathogenic microorganisms in concentrations up to 100 μM. The cytotoxic mycotoxin chaetochromin A [32] (**6**) on the other hand showed strong inhibition against MRSA with a MIC_{90} of 0.78 μM, which fits antibacterial activity against *S. aureus* reported in the literature [33]. Interestingly, compound **8** showed a moderate inhibition of *M. tuberculosis* with a MIC_{90} of 25 μM, whereas its carboxylic acid derivative (**7**) showed no inhibition even at 100 μM. The results are shown in Table 5.
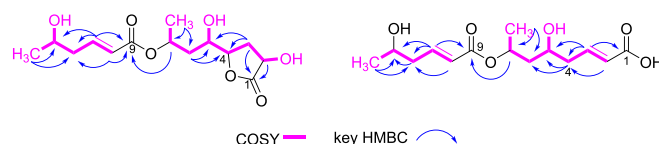
Table 4
NMR data for compounds **4** and **5** (measured in DMSO-d_6 at 150 Hz and 600 MHz, respectively).

Position	Compound [4]		Compound [5]	
	δ_C	δ_H, m (*J* in Hz)	δ_C	δ_H, m (*J* in Hz)
1*	177.0, C		167.2, C	
2	67.4, CH	4.45, dd (11.2, 8.1)	122.5, C	5.66, dd (15.7, 0.9)
2-OH		5.89, m		
3	32.8, CH_2	2.38, ddd (12.0, 8.6, 5.4)	149.3, CH	6.66, dd (15.7, 9.1)
		1.87, dt (12.0, 10.9)		
4	78.3, CH	4.21, dt (10.3, 5.1)	41.2, CH_2	2.37, ddd (15.7, 8.1, 3.7)
				2.26, m 3H
5	67.8, CH	3.51, q (4.5)	63.7, CH	3.37, dt (6.3, 3.6)
5-OH		5.19, d (5.7)		4.71, br s
6	38.3, CH_2	1.78, ddd (13.5, 9.3, 5.5)	36.2, CH_2	1.78, ddd (13.8, 9.7, 3.8)
		1.59, ddd (13.5, 8.1, 4.1)		1.54, ddd (13.9, 10.3, 3.5)
7	67.9, CH	5.04, dp (8.0, 6.3)	68.0, CH	4.79, dqd (9.7, 6.1, 3.4)
8	19.3, CH_3	1.22, d (6.2) 3H	20.1, CH_3	1.17, d (6.2)
9*	165.0, C		165.1, C	
10	122.7, CH	5.85, dt (15.6, 1.5)	122.1, CH	5.84, dt (15.6, 1.5)
11*	146.6, CH	6.89, dt (15.6, 7.3)	146.8, CH	6.89, dt (15.6, 7.3)
12	41.4, CH_2	2.25, m 2H	41.2, CH_2	2.26, m 3H
13	65.0, CH	3.74, h (6.1)	64.6, CH	3.75, m
13-OH		4.67, br s		not detected
14	23.4, CH_3	1.05, d (6.2) 3H	23.0, CH_3	1.06, d (6.2)

* Signals were extracted from HSQC and HMBC spectra.

Fig. 8. Key NMR correlations for compounds **4** (left) and **5** (right).

Table 5

MIC$_{90}$ against *S. aureus* ATCC 700699, *P. aeruginosa* ATCC 87110, *C. albicans* ATCC 24433 and *M. tuberculosis* H37Rv. All concentrations are shown in μM. Concentration > 100 μM indicates no activity in the experimental setup. Values represent means of experiments conducted in triplicates.

	MIC$_{90}$ [μM]			
Compound	*S. aureus* ATCC 700699	*P. aeruginosa* ATCC 87110	*C. albicans* ATCC 24433	*M. tuberculosis* ATCC 27294
1	>100	>100	>100	>100
2	>100	>100	>100	>100
3	>100	>100	>100	>100
4	>100	>100	>100	>100
5	>100	>100	>100	>100
6	0.78	>100	>100	>100
7	>100	>100	>100	>100
8	>100	>100	>100	25
9	>100	>100	>100	>100
10	>100	>100	>100	>100

2.3. Determination of cytotoxic activity

Compounds **1–10** were also tested for cytotoxic potential against the human monocytic cell line THP-1 using a resazurin assay. The mean IC$_{50}$ values are shown in Table 6. Compound **6** (chaetochromin A) had a strong cytotoxic effect with 0.7 μM which is similar to values described in the literature [32], while compound **8** (phenazin-1-carboxamide) had a weak cytotoxic effect with 42 μM on the THP-1 cell line. All remaining compounds including the five new compounds **1–5** showed no cytotoxic effect up to a concentration of 100 μM.

2.4. Proposed biosynthesis of linear colletodiol-derivatives

Structures of compounds **3–5** suggest that they represent direct precursors or alternative metabolites of the macrocyclic dilactones colletodiol and of close biosynthetic derivatives like colletol and colletoketol. It seems that this variation is related to one of the later biosynthetic steps, in which the closed ring form of the metabolites is being formed [34,35]. The last steps of the biosynthetic pathway of colletodiol and derivatives as proposed by O'Neill et al. [35] are presented in Fig. 9.

On the basis of the given information about the biosynthetic pathway of colletodiol and derivatives in *Cytospora* sp. from the literature [34,35], we propose a possible biosynthetic pathway in Fig. 10 that leads to the production of compounds **3–5**. However, it remains unclear whether the colletodiol biosynthetic pathways of *Cytospora* sp. and *Trichocladium* sp. are identical.

Table 6

IC$_{50}$ values of the isolated compounds **1–10** against human cell line THP1. All concentrations are shown in μM. Concentrations >100 μM indicate no activity in the experimental setup. Values represent means of experiments conducted in triplicates. IC$_{50}$ values were calculated using GraphPad Prism 7.

Compound	Mean IC$_{50}$ [μM]
1	>100
2	>100
3	>100
4	>100
5	>100
6	0.7
7	>100
8	42
9	>100
10	>100

3. Experimental section

3.1. General experimental procedures

Optical rotations were measured on a Jasco P-2000 polarimeter. UV-spectra were obtained using a Dionex P580 system in combination with a diode array detector (UVD340S) and an Eurosphere 10 C18 column (125 × 4 mm) with a flow rate of 1 ml/min. 1D and 2D NMR spectra were recorded on a Bruker Avance III (^{1}H, 600 MHz; ^{13}C 150 MHz) spectrometer. Mass spectra were obtained on a Finnigan LCQ Deca (Thermo Quest) mass spectrometer and for HRESIMS on a UHR-QTOF maXis 4G (Bruker Daltonics) mass spectrometer. Semipreperative HPLC was performed on a Lachrom-Merck Hitachi system (pump L7100, UV-detector L7400, Eurospher 100 C18 column, 300 × 8 mm, Knauer Germany) and a Knauer system (pump Azura P6.1L, autosampler Smartline 3950, UV-detector Smartline 2600, autocollector FOXY R1, column thermostat CT 2.1), respectively, with a flow rate of 5 ml/min. Precoated TLC silica gel 60 F254 plates (Merck) were used for tracking separation using detection under UV-light at 254 and 365 nm wavelengths or spraying with anisaldehyde-sulfuric acid reagent. VLC and non-vacuum-column chromatography was accomplished using Macherey Nagel silica gel 60 M (0.04–0.063 mm). Sephadex LH20 and RP18 was used as stationary phase for column chromatography. For the measurement of optical rotations, spectral grade solvents were used.

3.2. Fungal material

The isolation and identification of the endophytic fungus was described by Tran-Cong et al. [8]. Briefly, the fungus was isolated from the roots of the plant *Houttuynia cordata* (voucher specimen GOET038305, Göttingen University Herbarium) as an endophyte and was identified as *Trichocladium* sp. by sequencing of the ITS-sequence and data base comparison via the NCBI Blast tool (accession number MK241585). The voucher strain is deposited in the Institute of Pharmaceutical Biology and Biotechnology, Heinrich Heine University, Düsseldorf, Germany, under the code HCRSW.

3.3. Fermentation and extraction

Fermentation of the fungus was carried out in ten 1-l Erlenmeyer flasks using solid rice medium enriched with L-phenylalanine. For this, for each flask 2.5 g of phenylalanine were dissolved in 100 ml water and then added to 100 g of rice followed by autoclaving. Agar plates section of 1 × 1 cm^2 fungal material was inserted into each Erlenmeyer flask using a flame sterilised scalpel. The fungus was then grown for 21 days at 22 °C under static conditions. Each flask was extracted with 600 ml of EtOAc. The rice medium was cut into small pieces and shaken for 8 h followed by evaporation of the EtOAc.

3.4. Isolation

The crude extract (5.5 g) obtained from the fungal rice culture enriched with L-phenylalanine was seperated using a silica gel vacuum liquid chromatography (VLC). A step gradient of *n*-hexane/EtOAc and CH$_2$Cl$_2$/MeOH was used that yielded 16 fractions (V1-V16). Fractions V6 (510 mg) and V7 (53 mg) were combined and further purified using a LH20 sephadex column with MeOH as eluent giving nine subfractions (V6S1-V6S9). Subfraction V6S4 (31 mg) was conducted to semipreparative HPLC using a MeOH-H$_2$O step gradient from 58 to 78% MeOH to give **1** (0.8 mg), **8** (5.4 mg) and **9** (1 mg). Fractions V9 (792 mg), V10 (301 mg) and V11 (186 mg) were combined and then further separated by reverse-phase vacuum liquid chromatography using a step gradient of H$_2$O and MeOH, ranging from 0 to 100% MeOH, to give 7 subfractions (V9-11RP1-V9-11RP7). Subfractions V9-11RP1 (218 mg) and V9-11RP2 (146 mg) were purified similarly to V6S4 via semipreparative HPLC using MeOH-H$_2$O gradients of 5–50% MeOH and
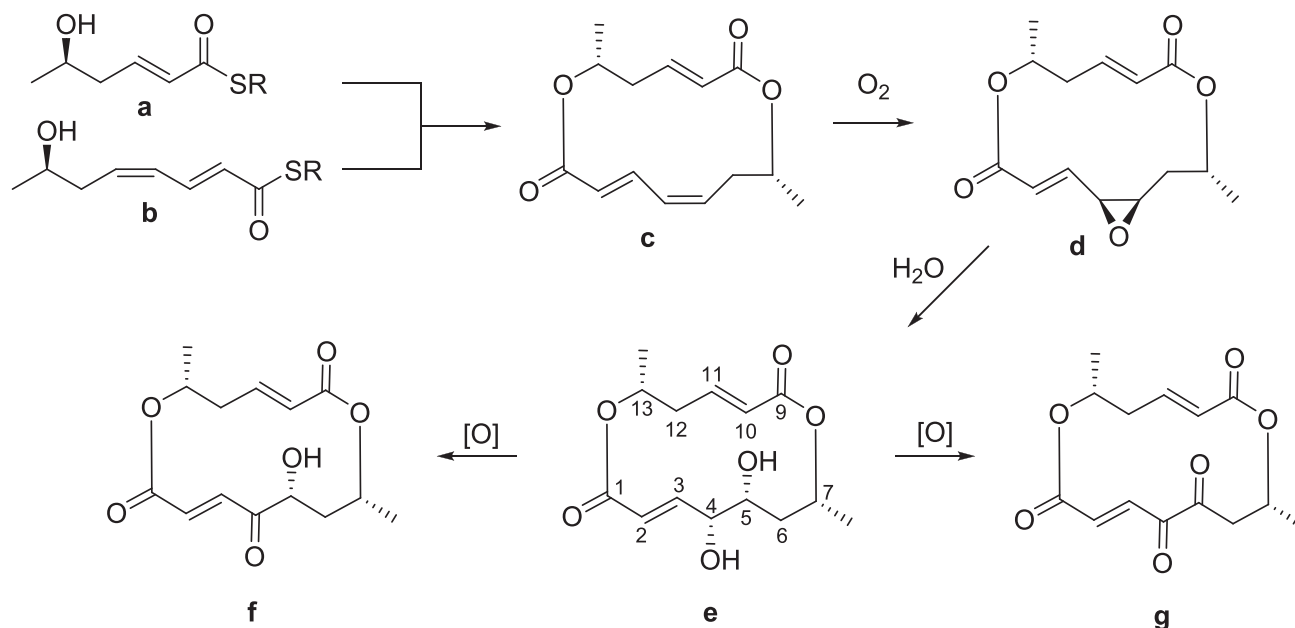
Fig. 9. Biosynthesis of colletodiol (**e**), colletoketol (**f**) and colletoketon (**g** = grahamimycin A1) from **a** and **b** as described by O'Neill et al. [35]. After cyclisation of **c**, an oxidative step introduces an epoxide group to form intermediate **d**. Hydrolysis of the epoxide leads to colletodiol, which can be oxidized to yield colletoketol and colletoketon.

30–56% MeOH respectively to yield **2** (3.4 mg), **3** (43.7 mg), **4** (5.4 mg), **5** (5.6 mg) and **10** (1.3 mg). Subfractions V4 (750 mg) and V5 (545 mg) were combined and conducted to silica column liquid chromatography using EtOAc as eluent followed by a step gradient of CH_2Cl_2/MeOH to give five subfractions (V4-5K1-V4-5K5). Subfraction V4—5K2 (207 mg) was purified by semi-preparative HPLC with a H_2O-MeOH step gradient from 50 to 80% MeOH giving **7** (3.4 mg). Subfraction V4—5K1 (221 mg) was transferred to a LH20 sephadex column using MeOH as eluent to yield **6** (106.9 mg).

3.4.1. Spectral data

Trichocladiol ((3S*,4R*)-3,4,6,8-tetrahydroxy-7-methyl-3,4-dihydronaphthalen-1(2H)-one - **compound 1**): white powder; $[\alpha]_D^{26}$–8.4 (c 0.225, MeOH); UV (MeOH) λ_{max} 291 nm; ^1H and ^{13}C NMR data, Table 1; HRESIMS m/z 225.0756 [M + H]$^+$ (calcd for $C_{11}H_{13}O_5$, 225.0757). Spectra are shown in supplementary materials **Fig. S3-S11**.

Trichocladic acid (2-((5,6-dimethyl-4-oxo-4H-pyran-2-yl)methyl)-4,6-dihydroxybenzoic acid – **compound 2**): white powder, UV (MeOH) λ_{max} 256 and 300 nm; ^1H and ^{13}C NMR data, Table 2; HRESIMS m/z 291.0866 [M + H]$^+$ and 313.0683 [M + Na]$^+$ (calcd for $C_{15}H_{15}O_6$, 291.0863 and $C_{15}H_{14}NaO_6$, 313.0680). Spectra are shown in supplementary materials **Fig. S12-S19**.

Colletodiolic acid ((E)-5-(((E)-4,5,7-trihydroxyoct-2-enoyl)oxy) hex-2-enoic acid – **compound 3**): colorless oil, $[\alpha]_D^{23}$ + 15.3 (c 1.0, MeOH), UV (MeOH) λ_{max} 218 nm; ^1H and ^{13}C NMR data, Table 3; HRESIMS m/z 303.1439 [M + H]$^+$, 320.1703 [M + NH$_4$]$^+$ and 325.1257 [M + Na]$^+$ (calcd for $C_{14}H_{23}O_7$, 303.1438; $C_{14}H_{26}NO_7$, 320.1704 and $C_{14}H_{22}NaO_7$, 325.1258). Spectra are shown in supplementary materials **Fig. S20-S28**.

Colletolactone (4-hydroxy-4-(4-hydroxy-5-oxotetrahydrofuran-2-yl)butan-2-yl (E)-5-hydroxyhex-2-enoate – **compound 4**): colorless oil, $[\alpha]_D^{22}$–18.4 (c 1.0, MeOH), UV (MeOH) λ_{max} 218 nm; ^1H and ^{13}C NMR data, Table 4; HRESIMS m/z 303.1442 [M + H]$^+$ and 320.1708 [M + NH$_4$]$^+$ (calcd for $C_{14}H_{23}O_7$, 303.1438 and $C_{14}H_{26}NO_7$, 320.1704). Spectra are shown in supplementary materials **Fig. S29-S37**.

Colletolic acid ((E)-5-hydroxy-7-(((E)-5-hydroxyhex-2-enoyl)oxy) oct-2-enoic acid – **compound 5**): colorless oil, $[\alpha]_D^{22}$–43.2 (c 1.0, MeOH), UV (MeOH) λ_{max} 219 nm; ^1H and ^{13}C NMR data, Table 4; HRESIMS m/z 287.1492 [M + H]$^+$ and 304.1759 [M + NH$_4$]$^+$ (calcd for

$C_{14}H_{23}O_6$, 287.1489 and $C_{14}H_{26}NO_6$, 304.1755). Spectra are shown in supplementary materials **Fig. S38-S46**.

Spectra for **compounds 6-10** are shown in supplementary materials **Fig. S47-S84**.

3.5. Media and strains

Nosocomial bacteria methicillin-resistant *Staphylococcus aureus* (MRSA) ATCC 700699 and *Pseudomonas aeruginosa* ATCC 87110 were grown in Mueller-Hinton-broth (MHB). The pathogenic yeast *Candida albicans* ATCC 24433 was grown in standard YPD medium (1% yeast extract, 2% peptone, and 2% glucose). The pathogenic bacterium *Mycobacterium tuberculosis* H37Rv (ATCC 27294) was grown in 7H9 supplemented with ADS (0.85% NaCl, 5% BSA, 2% dextrose), 0.5% glycerol, and 0.05% tyloxapol. Nosocomial bacteria and *C. albicans* were grown shaking at 120 rpm and 37 °C, *M. tuberculosis* was grown at 37 °C shaking at 80 rpm.

3.6. Determination of the minimal inhibitory concentration

Microbroth dilution assays were performed to determine the minimal inhibitory concentration (MIC$_{90}$) of compounds. Briefly, a serial 1:1 dilution of compounds was prepared in a 96-well round-bottom polystyrene plate in 50 μl growth medium ranging from 200 μM to 1.56 μM. The OD$_{600\ nm}$ of pre-grown bacterial cultures was determined, and a cell suspension in growth medium was adjusted to 10^6 CFU/ml. Afterwards, 50 μL of the cell suspension were added to each well thereby changing the compound concentration range to 100 μM to 0.78 μM. For MRSA ATCC 700699, *P. aeruginosa* ATCC 87110 and *C. albicans* ATCC 24433, the BacTiter Glo assay (Promega) was used to quantify growth after 24 h of incubation following the manufacturer's manual. Briefly, equal volumes of bacterial cell suspension and BacTiter Glo reagent were mixed in a white flat-bottom 96-well plate. After 5 min, luminescence was measured with a TECAN plate reader. Moxifloxacin was used as positive control for MRSA and *P. aeruginosa*, hygromycin was used as positive control for *C. albicans,* and DMSO was used as solvent control for all three organisms. For quantifying growth of *M. tuberculosis* H37Rv, the resazurin assay was used following a protocol as described previously [36]. Briefly, 10 μl of a 100 μg/ml resazurin solution were added to each
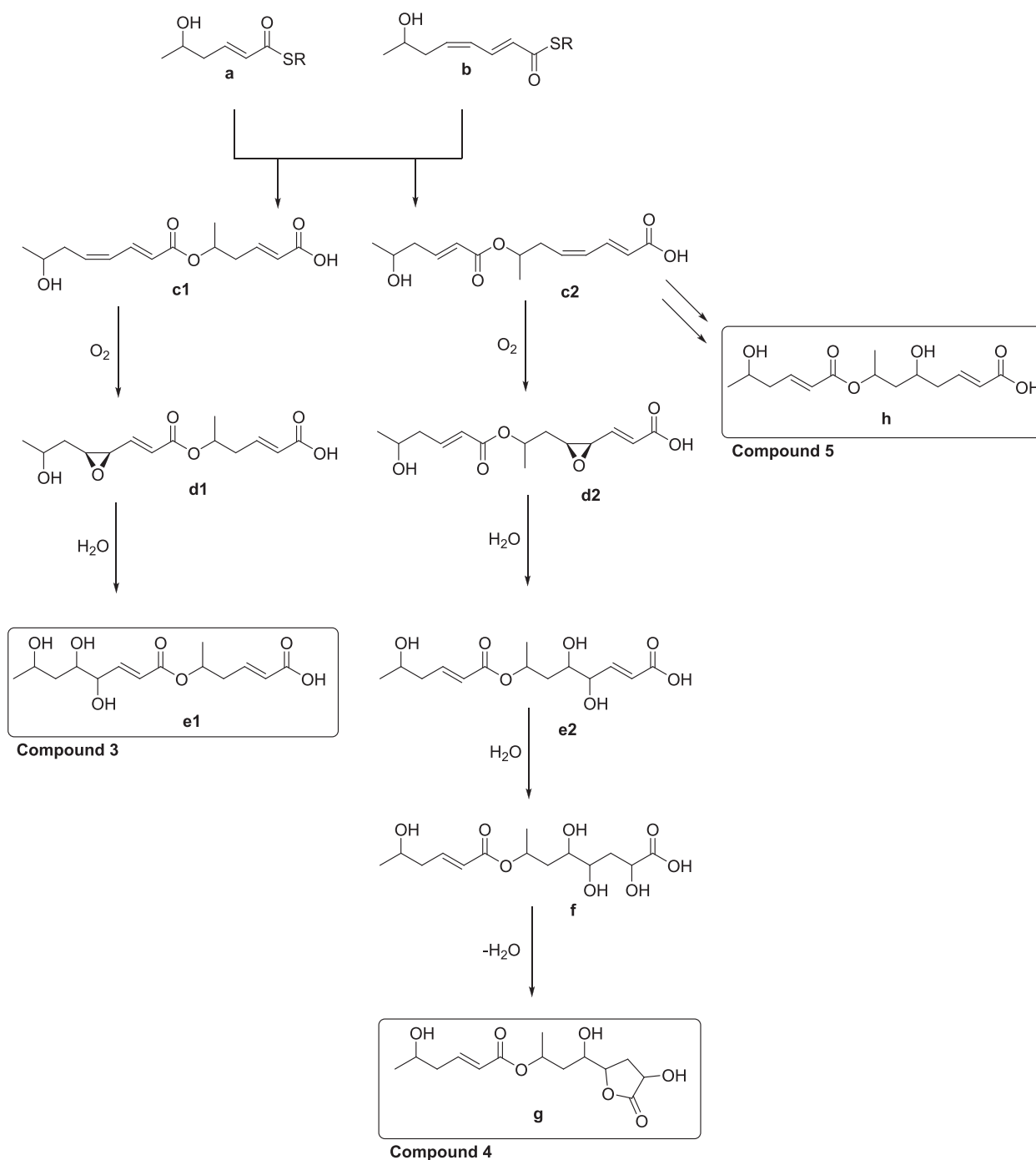
Fig. 10. Proposed biosynthesis to form compounds **3–5**. An alternative route starting from **a** and **b** results in the two different linear monoesters **c1** and **c2**. The following biosynthetic steps are likely similar to those of colletodiol biosynthesis, yielding **e1** (compound **3**) and **e2** over **d1** and **d2**. **g** (compound **4**) and **h** (compound **5**) might be formed from **e2** over **f** and **c2**, respectively, through undescribed metabolic steps.

well of the 96-well plate after five days of incubation at 37 °C, 5% CO$_2$, and in humified atmosphere. The plates were incubated for another 18 h at room temperature before stopping the reaction by the addition of 100 μl 10% formalin solution to each well. The fluorescence was measured at 535 nm excision and 590 nm emission using a Tecan Infinite 200pro microplate reader. Rifampicin and DMSO were used as positive and vehicle control, respectively. All experiments have been conducted in triplicates.

3.7. Determination of the cytotoxic activity against THP-1 cells

The cytotoxicity assay was performed using THP-1 cells (human monocytic leukaemia cell line) in a procedure described before [37]. The cells were cultivated in RPMI 1640 medium containing 2 mM L-glutamine and supplemented with 10% fetal calf serum (FCS) and 1% sodium pyruvate at 37 °C in an atmosphere of 5% CO$_2$. Cells were adjusted to a density of 2×10^5 cells/ml, and 50 μl of this suspension was transferred per well to 96-well flat bottom microtiter plates containing 2-fold serial dilutions of the tested compounds resulting in final concentrations ranging from 100 to 0.78 μM in a total volume of 100 μL.

Cycloheximide at concentrations of 4 to 0.03 μg/ml was used as positive control. The cells were then incubated for 48 h at 37 °C in a humidified atmosphere with 5% CO_2. Subsequently, 10 μL of a resazurin solution (100 μg/ml) were added to each well, followed by another incubation step for 4 h. The fluorescence was quantified using a Tecan Infinite 200pro microplate reader (excitation 540 nm, emission 590 nm). The residual growth was calculated relative to non-inoculated (0% growth) and controls treated with DMSO (100% growth), respectively.

3.8. Computational section

Mixed torsional/low-mode conformational searches were carried out by means of the Macromodel 10.8.011 software using the MMFF with an implicit solvent model for $CHCl_3$ applying a 21 kJ/mol energy window [38]. Geometry re-optimizations of the resultant conformers (ωB97X/ TZVP PCM/MeOH) and TDDFT ECD calculations were performed with Gaussian 09 using various functionals (B3LYP, BH&HLYP, CAMB3LYP, PBE0) and the TZVP basis set with the same solvent model as in the preceding DFT optimization step [39]. ECD spectra were generated as the sum of Gaussians with 3000 cm^{-1} half-height width, using dipole-velocity-computed rotational strength values [40]. Boltzmann distributions were estimated from the ωB97X energies. The MOLEKEL program was used for visualization of the results [41].

CRediT authorship contribution statement

Viktor E. Simons: Conceptualization, Investigation, Writing – original draft. **Attila Mándi:** Investigation, Writing – review & editing. **Marian Frank:** Data curation. **Lasse van Geelen:** Investigation. **Nam Tran-Cong:** Data curation. **Dorothea Albrecht:** Investigation. **Annika Coort:** Investigation. **Christina Gebhard:** Investigation. **Tibor Kurtán:** Data curation, Formal analysis, Funding acquisition, Writing – original draft, Writing – review & editing, Supervision. **Rainer Kalscheuer:** Conceptualization, Data curation, Funding acquisition, Project administration, Supervision, Writing – original draft, Writing – review & editing.

Declaration of competing interest

None to declare.

Acknowledgments

Appendix A. Supplementary data

Supplementary data to this article can be found online at https://doi. org/10.1016/j.fitote.2024.105914.

References

[1] A. Fleming, On the antibacterial action of cultures of a Penicillium, with special reference to their use in the isolation of B. Influenza, Br. J. Exp. Pathol. 10 (1929) 226–236.

[2] S.A. Waksman, H.B. Woodruff, The soil as a source of microorganisms antagonistic to disease-producing bacteria, J. Bacteriol. 40 (1940) 581–600, https://doi.org/10.1128/jb.40.4.581-600.1940.

[3] A. Stierle, G. Strobel, D. Stierle, Taxol and taxane production by Taxomyces andreanae, an endophytic fungus of Pacific yew, Science 260 (1993) 214–216, https://doi.org/10.1126/science.8097061.

[4] G.A. Strobel, Endophytes as sources of bioactive products, Microbes Infect. 5 (2003) 535–544, https://doi.org/10.1016/s1286-4579(03)00073-x.

[5] R.P. Ryan, K. Germaine, A. Franks, D.J. Ryan, D.N. Dowling, Bacterial endophytes: recent developments and applications, FEMS Microbiol. Lett. 278 (2008) 1–9, https://doi.org/10.1111/j.1574-6968.2007.00918.x.

[6] P.J. Rutledge, G.L. Challis, Discovery of microbial natural products by activation of silent biosynthetic gene clusters, Nat. Rev. Microbiol. 13 (2015) 509–523, https://doi.org/10.1038/nrmicro3496.

[7] H.B. Bode, B. Bethe, R. Höfs, A. Zeeck, Big effects from small changes: possible ways to explore nature's chemical diversity, ChemBioChem 3 (2002) 619–627.

[8] N.M. Tran-Cong, A. Mándi, T. Kurtán, W.E.G. Müller, R. Kalscheuer, W. Lin, Z. Liu, P. Proksch, Induction of cryptic metabolites of the endophytic fungus Trichocladium sp. through OSMAC and co-cultivation, RSC Adv. 9 (2019) 27279–27288, https://doi.org/10.1039/c9ra05469c.

[9] K. Koyama, S. Natori, Y. Iitaka, Absolute configurations of chaetochromin a and related bis(naphtho-gamma-pyrone) mold metabolites, Chem. Pharm. Bull. 35 (1987) 4049–4055. DOI: 10.1248.

[10] S. Mehnaz, R.S. Saleem, B. Yameen, I. Pianet, G. Schnakenburg, H. Pietraszkiewicz, F. Valeriote, M. Josten, H.G. Sahl, S.G. Franzblau, H. Gross, Lahorenoic acids A-C, ortho-dialkyl-substituted aromatic acids from the biocontrol strain Pseudomonas aurantiaca PB-St2, J. Nat. Prod. 76 (2013) 135–141, https://doi.org/10.1021/np3005166.

[11] R.S. Kumar, N. Ayyadurai, P. Pandiaraja, A.V. Reddy, Y. Venkateswarlu, O. Prakash, N. Sakthivel, Characterization of antifungal metabolite produced by a new strain Pseudomonas aeruginosa PUPa3 that exhibits broad-spectrum antifungal activity and biofertilizing traits, J. Appl. Microbiol. 98 (2005) 145–154, https://doi.org/10.1111/j.1365-2672.2004.02435.x.

[12] M. Yu, B.B. Snider, Syntheses of chloroisosulochrin and isosulochrin and biomimetic elaboration to maldoxin, maldoxone, dihydromaldoxin, and dechlorodihydromaldoxin, Org. Lett. 13 (2011) 4224–4227, https://doi.org/10.1021/ol201561w.

[13] B.K. Joshi, J.B. Gloer, D.T. Wicklow, Bioactive natural products from a sclerotium-colonizing isolate of Humicola fuscoatra, J. Nat. Prod. 65 (2002) 1734–1737, https://doi.org/10.1021/np020295p.

[14] A.R. Ola, D. Thomy, D. Lai, H. Brotz-Oesterhelt, P. Proksch, Inducing secondary metabolite production by the endophytic fungus fusarium tricinctum through coculture with Bacillus subtilis, J. Nat. Prod. 76 (2013) 2094–2099, https://doi.org/10.1021/np400589h.

[15] J. Fungal MacMillan, Part V. Products, The absolute stereochemistry of Colletodiol and the structures of related metabolites of Colletotrichum capsici, J.C.S. 3 (1973) 1487–1493.

[16] J.F. Grove, Metabolic Products of Colletotrichum capsici. Isolation and characterisation of Acetylcolletotrichin and Colletodiol, J. Chem. Soc. 5 (1966) 230–234.

[17] K. Ohta, O. Mitsunobu, Formal total synthesis of grahamimycin A1, Tetrahedron Lett. 32 (1991) 517–520.

[18] T.A.S. Kurtan, G. Pescitelli, Electronic CD of benzene and other aromatic chromophores for determination of absolute configuration. Comprehensive Chiroptical, Spectroscopy 2 (2012) 73–114.

[19] G.S.F. Snatzke, Chiroptische Methoden, Springer-Verlag, 1980.

[20] J.M. Hu, J.J. Chen, J. Yu, H.Y.X. Zhao, J. Zhou, Five new compounds from Dendrobium longicornu, Planta Med. 74 (2008) 535–539, https://doi.org/10.1055/s-2008-1074492.

[21] D. Slade, D. Ferreira, J.P. Marais, Circular dichroism, a powerful tool for the assessment of absolute configuration of flavonoids, Phytochemistry 66 (2005) 2177–2215, https://doi.org/10.1016/j.phytochem.2005.02.002.

[22] E. Couche, A. Fkyerat, R. Tabacchi, Asymmetric synthesis of the cis- and trans-3,4-dihydro-2,4,8-trihydroxynaphthalen-1(2H)-ones, Helv. Chim. Acta 86 (2003) 210–221, https://doi.org/10.1002/hlca.200390014.

[23] D.G. Laurent, A new cytotoxic tetralone derivative from Humicola grisea, a filamentous fungus from wood in the southeastern lagoon of New Caledonia, Tetrahedron 58 (2002) 9163–9167.

[24] L. Liu, A.L. Li, M.B. Zhao, P.F. Tu, Tetralones and flavonoids from Pyrola calliantha, Chem. Biodivers. 4 (2007) 2932–2937, https://doi.org/10.1002/cbdv.200790242.

[25] L.T.K. Kagawa, K. Uchida, H. Kakushi, T. Shike, H. Nakai, Platelet aggregation inhibitors and inotropic constituents in Pyrolae Herba, Chem. Pharm. Bull. 40 (1992) 2083–2087.

[26] G. Bringmann, K. Messer, W. Saeb, E.M. Peters, K. Peters, The absolute configuration of (+)-isoshinanolone and in situ LC-CD analysis of its stereoisomers from crude extracts, Phytochemistry 56 (2001) 387–391, https://doi.org/10.1016/s0031-9422(00)00386-1.

[27] N. Allouche, B. Morleo, O. Thoison, V. Dumontet, O. Nosjean, F. Gueritte, T. Sevenet, M. Litaudon, Biologically active tetralones from new Caledonian Zygogynum spp, Phytochemistry 69 (2008) 1750–1755, https://doi.org/10.1016/j.phytochem.2008.01.025.

[28] S. Superchi, P. Scafato, M. Gorecki, G. Pescitelli, Absolute configuration determination by quantum mechanical calculation of Chiroptical spectra: basics and applications to fungal metabolites, Curr. Med. Chem. 25 (2018) 287–320, https://doi.org/10.2174/0929867324666170310112009.

[29] A. Mándi, T. Kurtán, Applications of OR/ECD/VCD to the structure elucidation of natural products, Nat. Prod. Rep. 36 (2019) 889–918, https://doi.org/10.1039/c9np00002j.

[30] H. Li, Z.B. Liao, D. Tang, W.B. Han, Q. Zhang, J.M. Gao, Polyketides from two species and their biological functions, J. Antibiot. 71 (2018) 677–681, https://doi.org/10.1038/s41429-018-0047-x.

[31] J. MacMillan, R.J. Pryce, The structure of colletodiol, a macrocyclic dilactone from Colletotrichum capsici, Tetrahedron Lett. 9 (1968) 5497–5500. DOI: 10.1016.

[32] K. Koyama, K. Ominato, S. Natori, T. Tashiro, T. Tsuruo, Cytotoxicity and antitumor activities of fungal bis(naphtho-gamma-pyrone) derivatives, Aust. J. Pharm. 11 (1988) 630–635, https://doi.org/10.1248/bpb1978.11.630.

[33] G.B. Xu, T. Yang, J.K. Bao, D.M. Fang, G.Y. Li, Isochaetomium A2, a new bis (naphthodihydropyran-4-one) with antimicrobial and immunological activities from fungus Chaetomium microcephalum, Arch. Pharm. Res. 37 (2014) 575–579, https://doi.org/10.1007/s12272-013-0206-3.

[34] J. Simpson, Studies of polyketide chain assembly processes. Origins of the hydrogen and oxygen atoms in Colletodiol, J. Chem. Soc. Chem. Commun. (1985) 1822–1824.

[35] J.A. O'Neill, Biosynthesis of Colletodiol and Related polyketide Macrodiolides in Cytospora sp. ATCC 20502: Synthesis and Metabolism of Advanced Intermediates, J. Chem. Soc. Chem. Commun., 1993.

[36] N. Rehberg, E. Omeje, S.S. Ebada, L. van Geelen, Z. Liu, P. Sureechatchayan, M. U. Kassack, T.R. Ioerger, P. Proksch, R. Kalscheuer, 3-O-methyl-Alkylgallates

[37] D. Meier, M.V. Hernandez, L. van Geelen, R. Muharini, P. Proksch, J.E. Bandow, R. Kalscheuer, The plant-derived chalcone Xanthoangelol targets the membrane of gram-positive bacteria, Bioorg. Med. Chem. 27 (2019) 115151, https://doi.org/10.1016/j.bmc.2019.115151.

[38] MacroModel, Schrödinger, 2015. Available online, http://www.schrödinger.com/MacroModel.

[39] M.K.T.G.W. Frisch, H.B. Schlegel, G.E. Scuseria, M.A. Robb, J.R. CHeeseman, G. Scalmani, V. Barone, B. Mennucci, G.A. Petersson, Gaussian 09, Revision E.01, Gaussian, Inc., Wallingford, CT, USA, 2013.

[40] P.J. Stephens, N. Harada, ECD cotton effect approximated by the Gaussian curve and other methods, Chirality 22 (2010) 229–233, https://doi.org/10.1002/chir.20733.

[41] U. Varetto, Molekel 5.4, Swiss National Supercomputing Centre, Manno, Switzerland, 2009.

inhibit fatty acid desaturation in mycobacterium tuberculosis, Antimicrob. Agents Chemother. 63 (2019), https://doi.org/10.1128/AAC.00136-19.